Parabolized Stability Analysis of Jets Issuing from Serrated Nozzles

Aniruddha Sinha[1], Hao Xia[2] & Tim Colonius[3]
[1] *Aerospace Engineering, Indian Institute of Technology Bombay, Mumbai, 400076, INDIA*
[2] *Aeronautical Engineering, Loughborough University, Leicestershire LE11 3TU, UK*
[3] *Engineering and Applied Sciences, California Institute of Technology, Pasadena, CA, USA*
E-mail: as@aero.iitb.ac.in

1 Introduction

Large-scale coherent structures have been detected in unforced high-speed turbulent jets issuing from round nozzles several decades ago, starting with the pioneering work of Mollo-Christensen (1967), Crow & Champagne (1971). Since then, researchers have proposed models for these structures, mostly based on hydrodynamic stability analysis of the turbulent mean flow field (Mankbadi & Liu 1984, Tam & Chen 1994, Balakumar 1998, Yen & Messersmith 1998, Piot et al. 2006). More recent work by Suzuki & Colonius (2006), Gudmundsson & Colonius (2011), Cavalieri et al. (2013), Sinha et al. (2014) have presented detailed validation results for this model by suitable filtering of the wealth of flow data that has become available, both from experiments and from large-eddy simulation (LES).

The essential hypothesis of the theory is that coherent structures account for a small fraction of the turbulent kinetic energy (demonstrated by (Cavalieri et al. 2013)), and therefore have linear dynamics. They can be said to reside on top of the time-averaged mean flow field. The incoherent, or fine-scale, structure of turbulence, although essential for establishing the mean field through the energy cascade, is not directly interacting with the large-scale structures. Recent reviews by Jordan & Gervais (2008), Jordan & Colonius (2013) articulate this conjecture.

2 Linear Parabolized Stability Equations for Jets Issuing from Serrated Nozzles

We formulate the linear parabolized stability equations (PSE) for viscous compressible jets with a serrated mean flow field. The usual compressible formulation is used to nondimensionalize flow quantities. Linear dimensions are normalized by the nozzle exit diameter D, velocities by the ambient speed of sound c_∞, density by the ambient density ρ_∞, and pressure by $\rho_\infty c_\infty^2$. Time is normalized by D/c_∞. However, for the purposes of reporting, frequency is normalized by U_j/D to the more common Strouhal number St, where U_j is the nozzle exit velocity. The acoustic Mach number of the jet is $M_a = U_j/c_\infty$, whereas the jet exit Mach number is $M_j = U_j/c_j$, with c_j being the speed of sound at the nozzle exit. The jet exit Reynolds number is $Re_j = \rho_j U_j D/\mu_j$, with ρ_j and μ_j being respectively the density and viscosity at the nozzle exit. In the stability analysis, the temperature dependence of viscosity is ignored since the temperature ratio of the jets considered is close to unity. Moreover, the Prandtl number Pr is fixed at 0.7 for air.

The jet flow field is described in cylindrical coordinates (x, r, θ) by $\boldsymbol{q} = (u_x, u_r, u_\theta, p, \zeta)^{\mathrm{T}}$, which respectively denote the axial, radial and azimuthal components of velocity, pressure and specific volume. The instantaneous flow field is decomposed as fluctuations $\boldsymbol{q}'$ of the time-averaged turbulent flow field $\overline{\boldsymbol{q}}$, i.e. $\boldsymbol{q}(x, r, \theta, t) = \overline{\boldsymbol{q}}(x, r, \theta) + \boldsymbol{q}'(x, r, \theta, t)$. The mean pressure is constant in the free jets under consideration, and its non-dimensional value is $1/\gamma$, γ being the ratio of the specific heats (assumed 1.4).

The corrugated mean flow has symmetries in the θ-domain, that may be exploited advantageously. We start by defining the mth azimuthal Fourier mode of, say $T(\theta)$, as $\hat{T}_m := (1/2\pi)\int_{-\pi}^{\pi} T(\theta)\,\mathrm{e}^{-\mathrm{i}m\theta}\mathrm{d}\theta$. Our nozzle has L chevrons distributed *uniformly* around the circumference (e.g., $L = 6$ in SMC001). The resulting turbulent mean flow field has an L-fold rotational symmetry so that $\hat{\overline{\boldsymbol{q}}}_m$ vanishes for all m that are *not* integer multiples of L. Moreover, the chevrons are usually mirror-symmetric about their tip (and root) center planes,

so that the mean flow field may be written as

$$\overline{\boldsymbol{q}}\left(x,r,\theta\right)=\sum_{j=0}^{\infty}\hat{\overline{\boldsymbol{q}}}_{Lj}\left(x,r\right)\cos\left(Lj\theta\right), \tag{1}$$

as long as θ is measured from such a plane of mirror symmetry (which is assumed to be case here). Note that $\hat{\overline{\boldsymbol{q}}}$ is a real field.

The set of five governing equations for the viscous compressible flow linearized about the serrated mean flow field $\overline{\boldsymbol{q}}$ are compactly represented in matrix form as

$$\left\{\overline{\mathcal{L}}^{0}+\overline{\mathcal{L}}^{t}\frac{\partial}{\partial t}+\overline{\mathcal{L}}^{x}\frac{\partial}{\partial x}+\overline{\mathcal{L}}^{r}\frac{\partial}{\partial r}+\overline{\mathcal{L}}^{\theta}\frac{\partial}{\partial\theta}+\overline{\mathcal{L}}^{xx}\frac{\partial^{2}}{\partial x^{2}}+\overline{\mathcal{L}}^{rr}\frac{\partial^{2}}{\partial r^{2}}+\overline{\mathcal{L}}^{\theta\theta}\frac{\partial^{2}}{\partial\theta^{2}}+\overline{\mathcal{L}}^{xr}\frac{\partial^{2}}{\partial x\partial r}+\overline{\mathcal{L}}^{r\theta}\frac{\partial^{2}}{\partial r\partial\theta}+\overline{\mathcal{L}}^{\theta x}\frac{\partial^{2}}{\partial\theta\partial x}\right\}\boldsymbol{q}'=\boldsymbol{0}. \tag{2}$$

The 5×5 coefficient matrices $\overline{\mathcal{L}}$ are linear functions of $\overline{\boldsymbol{q}}$, and are parametrized by Re_j, M_a and Pr.

Since the coefficient matrices in eqn. (2) do not depend on time, the solution is separable into its various constituent frequencies (normal modes)

$$\boldsymbol{q}'\left(x,r,\theta,t\right)=\breve{\boldsymbol{q}}_{\omega}\left(x,r,\theta\right)\mathrm{e}^{-\mathrm{i}\omega t}+\text{c.c.}, \tag{3}$$

where, $\omega=2\pi StM_a$ is the angular frequency. In round jets, the solution may also be separated into individual azimuthal modes owing to the axisymmetric mean flow field (Gudmundsson & Colonius 2011). However, this isn't possible a priori for a serrated mean flow, and instead we write the normal mode $\breve{\boldsymbol{q}}_{\omega}$ as

$$\breve{\boldsymbol{q}}_{\omega}\left(x,r,\theta\right)=\sum_{m=-\infty}^{\infty}\hat{\breve{\boldsymbol{q}}}_{\omega,m}\left(x,r\right)\mathrm{e}^{\mathrm{i}m\theta}. \tag{4}$$

For the convectively unstable flows under consideration, the PSE model assumes that the mode shape $\hat{\breve{\boldsymbol{q}}}$ can be further decomposed into a rapidly varying streamwise wave-like component modulated by a function with streamwise variations on the order of the (slowly-varying) base flow:

$$\hat{\breve{\boldsymbol{q}}}_{\omega,m}\left(x,r\right)=B_{\omega}\,\tilde{\boldsymbol{q}}_{\omega,m}\left(x,r\right)\chi_{\omega}\left(x\right),\qquad\chi_{\omega}\left(x\right)=\exp\left\{\mathrm{i}\int_{x_0}^{x}\alpha_{\omega}\left(\xi\right)\mathrm{d}\xi\right\}. \tag{5}$$

Here, $\tilde{\boldsymbol{q}}_{\omega,m}$ is a shape function and α_{ω} is a complex axial wavenumber, both assumed to have mild axial variation. Also, B_{ω} is a complex scalar that sets the absolute amplitude and phase of the PSE solution. Note that the coupling of the various azimuthal modes in the solution dictates that α and B are common across all azimuthal modes, and only the shape functions $\tilde{\boldsymbol{q}}$ are different for each m (this perspective will be refined subsequently).

With the ansatz as per eqn. (5), the first and second x-derivatives of the mode shape $\hat{\breve{\boldsymbol{q}}}$ are

$$\frac{\partial\hat{\breve{\boldsymbol{q}}}}{\partial x}=\left(\mathrm{i}\alpha\tilde{\boldsymbol{q}}+\frac{\partial\tilde{\boldsymbol{q}}}{\partial x}\right)\chi,\qquad\frac{\partial^{2}\hat{\breve{\boldsymbol{q}}}}{\partial x^{2}}=\left(-\alpha^{2}\tilde{\boldsymbol{q}}+\mathrm{i}\frac{\partial\alpha}{\partial x}\tilde{\boldsymbol{q}}+2\mathrm{i}\alpha\frac{\partial\tilde{\boldsymbol{q}}}{\partial x}\right)\chi, \tag{6}$$

where $\partial^2\tilde{\boldsymbol{q}}/\partial x^2$ is neglected on account of the slow-variation assumption.

Substituting the foregoing ansatz in the linearized governing equations eqn. (2), we obtain

$$\sum_{j=-\infty}^{\infty}\left[\hat{\overline{\mathcal{L}}}_{Lj}^{0}-\mathrm{i}\omega\hat{\overline{\mathcal{L}}}^{t}+\hat{\overline{\mathcal{L}}}_{Lj}^{r}\frac{\partial}{\partial r}+\hat{\overline{\mathcal{L}}}_{Lj}^{rr}\frac{\partial^{2}}{\partial r^{2}}+\mathrm{i}\left(m-Lj\right)\left(\hat{\overline{\mathcal{L}}}_{Lj}^{\theta}+\hat{\overline{\mathcal{L}}}_{Lj}^{r\theta}\frac{\partial}{\partial r}\right)-\left(m-Lj\right)^{2}\hat{\overline{\mathcal{L}}}_{Lj}^{\theta\theta}+\left\{\hat{\overline{\mathcal{L}}}_{Lj}^{x}+\hat{\overline{\mathcal{L}}}_{Lj}^{xr}\frac{\partial}{\partial r}+\mathrm{i}\left(m-Lj\right)\hat{\overline{\mathcal{L}}}_{Lj}^{\theta x}\right\}\left(\mathrm{i}\alpha+\frac{\partial}{\partial x}\right)+\hat{\overline{\mathcal{L}}}_{Lj}^{xx}\left(-\alpha^{2}+\mathrm{i}\frac{\partial\alpha}{\partial x}+2\mathrm{i}\alpha\frac{\partial}{\partial x}\right)\right]\tilde{\boldsymbol{q}}_{\omega,m-Lj}=\boldsymbol{0}. \tag{7}$$

Here, the operator $\hat{\overline{\mathcal{L}}}_m$ is the mth azimuthal mode of the corresponding operator $\overline{\mathcal{L}}$ in eqn. (2), and it inherits the sparsity of the serrated mean flow field representation in eqn. (1). Note that the neglect of $\partial^2\tilde{\boldsymbol{q}}/\partial x^2$ renders the equations approximately parabolic for convectively-unstable flows such as the jet under consideration (Li & Malik 1997).

Equation (7) indicates that a given azimuthal mode, say $\tilde{\boldsymbol{q}}_l$, is only coupled with other azimuthal modes in the set $\{\tilde{\boldsymbol{q}}_{l-Lk}\}_{k=-\infty}^{\infty}$. Evidently, there are only L unique sets of this kind, each of which represents a

separable solution of eqn. (7). We index these sets by the lowest azimuthal mode appearing in them; i.e., $\tilde{\boldsymbol{Q}}^M := \{\tilde{\boldsymbol{q}}_{M-Lk}\}_{k=-\infty}^{\infty}$, for $-L/2 < M \leq L/2$. We term the set $\tilde{\boldsymbol{Q}}^M$ as the Mth 'azimuthal order' of the PSE solution. These azimuthal orders also represent the L separable normal mode solutions:

$$\breve{\boldsymbol{q}}_\omega^M(x,r,\theta) = B_\omega^M \sum_{j=-\infty}^{\infty} \tilde{\boldsymbol{q}}_{\omega,M-Lj}(x,r) \exp\left[\mathrm{i}\left\{(M-Lj)\,\theta + \int_{x_0}^{x} \alpha_\omega^M(\xi)\,\mathrm{d}\xi\right\}\right]. \tag{8}$$

The dense m-coupling implied by eqn. (4) is therefore clarified to be a set of sparse couplings, with separate streamwise wavenumber $\alpha_\omega^M(x)$ and overall amplitudes B_ω^M. As in all linear stability theory, the governing equation (eqn. (7)) is homogenous, so that it neither depends on nor predicts the absolute amplitude B_ω^M in eqn. (5). The decomposition in eqn. (5) is ambiguous since the axial variation can be subsumed in either $\tilde{\boldsymbol{q}}$ or α. Following Herbert (1997), the following normalization constraint is prescribed

$$\int_0^\infty \sum_{j=-\infty}^{\infty} \tilde{\boldsymbol{q}}_{\omega,M-Lj}^\dagger \mathcal{W} \frac{\partial \tilde{\boldsymbol{q}}_{\omega,M-Lj}}{\partial x} r\mathrm{d}r = 0, \tag{9}$$

where $(\cdot)^\dagger$ denotes the complex conjugate transpose, and the weight matrix $\mathcal{W} := \mathrm{diag}(1,1,1,0,0)$. This aims to remove any exponential dependence on x from the shape function $\tilde{\boldsymbol{q}}$ (in the sense of a TKE norm).

The infinite sums in the azimuthal modal domain indicated above must be truncated in the computation. We assume that the azimuthal complexity of $\overline{\boldsymbol{q}}(r,\theta)$ is such that the summation in eqn. (1) can be truncated to $\pm J$. For the calculations presented herein, $J = 2$ was found to be adequate. Since the matrices $\overline{\mathcal{L}}$ are linear functions of $\overline{\boldsymbol{q}}$, the summation in eqn. (7) is also truncated to $\pm J$. The summation in eqn. (8) (and hence the degree of azimuthal coupling in eqn. (7)) is also truncated to $\pm N$ ($\geq J$). The rationale is that high azimuthal modes tend to have negligible impact on the dynamics of the low azimuthal modes, which are most unstable in general. Converged solutions are found in the present calculations with $N = 7$.

Since the mean flow loses its serrated character far enough away from the control devices, the individual azimuthal modes in eqn. (7) decouple at $r \to \infty$. Thus, we use characteristic boundary conditions (Thompson 1987) to close the outer domain at $r = 10$, as in a round jet (Gudmundsson & Colonius 2011). The centerline behavior of each azimuthal mode is formulated as a Fourier azimuthal counterpart of the pole condition proposed by Mohseni & Colonius (2000) (see also Sinha et al. (2014)).

The radial grid is clustered near the lip-line using an `erf` mapping (Freund 1997). With 500 grid points, the minimum spacing is $\Delta r = 0.0051$. Fourth-order central difference is used to discretize the radial derivative operators. First-order implicit Euler differences are used to approximate the streamwise derivatives, and this results in a system of linear equations to solve for the shape functions at each axial position, given a guess for α_ω^M. The latter is solved for iteratively to satisfy eqn. (9), as shown by Day et al. (2001). The sparsity of the linear system of equations is exploited in the solution by the MUMPS library (Amestoy et al. 2001).

For stable downstream march of the solution, Li & Malik (1997) specify the following lower bound on the axial step-size

$$\Delta x \geq \frac{1}{\left|\mathrm{Re}\left\{\alpha_\omega^M(x)\right\}\right|}. \tag{10}$$

An upstream condition (akin to the initial condition for time marching) is required to begin the axial march at $x = x_0$. This is obtained by solving the classical parallel-flow linear stability problem based on the mean flow profile close to the nozzle exit, and extracting the Kelvin-Helmholtz (K-H) mode.

3 Large-eddy simuation database

The LES database used in this work was developed to simulate the SMC001 chevron nozzle at $M_a = 0.9$ and $T_j/T_\infty = 0.84$, with $Re_j = 1.03 \times 10^6$ (the 'SP7' case in the database of Tanna (1977)). The first simulation reported by Xia et al. (2009) had 12.5 million grid cells, but the resolution has since been improved to X million grid cells. The numerical scheme is a hybrid of implicit LES coupled with Spalart-Almaras near-wall RANS modeling. The flow solver, FLUXp, is based on a cell-centered finite volume discretization for arbitrarily unstructured meshes. However, hexahedral body-fitted meshes with conformed multi-block structured topologies are used to avoid cell skewness around the challenging chevron geometry. The simulation time step is $5 \times 10^{-4} D/U_j$, and it is run for a time duration of $200 D/U_j$ beyond the initial transients. Xia et al. (2009) demonstrated favorable agreement of the mean velocity and Reynolds stresses with the NASA experimental data.

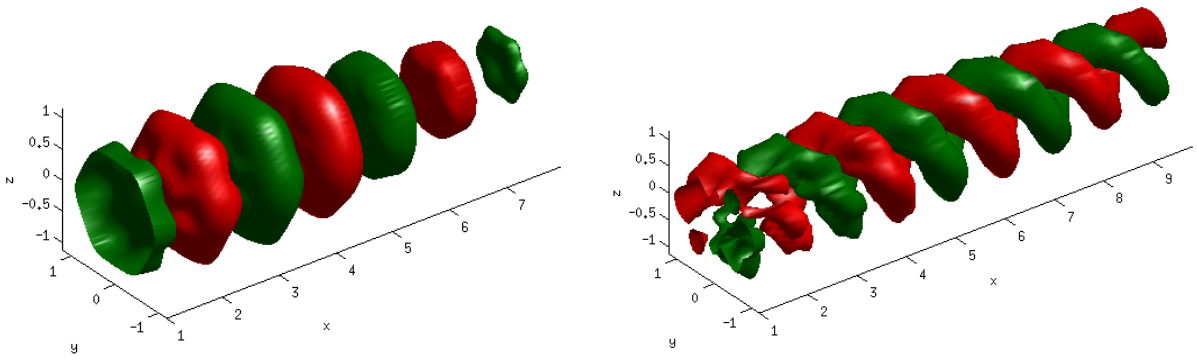

(a) (b)

Figure 1: Representative positive and negative isosurfaces of the real part of pressure in the PSE solution for $St = 0.3$ corresponding to azimuthal orders (a) $M = 0$, and (b) $M = 1$.

For the purpose of the present validation, the simulation data is acquired at 225 axial planes in $0 \leq x \leq 20$, with spacing increasing downstream in geometrical progression. The cross-stream domain was sampled using a polar grid having 200 radial grid points in $0 \leq r \leq 5$, with clustering near the lip-line. The uniform azimuthal grid had 120 points. The pre-processing of the mean flow field is described in Appendix A.

The LES fluctuation data must be transformed to the frequency domain for comparison with the LST normal modes. To obtain statistically significant results, the LES time-series (which was sampled at intervals of $0.02D/U_j$) was first divided into 75%-overlapping Hann-windowed segments. For estimating the $St = 0.2$ mode, each segment length was chosen to be sufficient for resolving 1/4th of this frequency (i.e., it was $20D/U_j$ long). Thirty six such segments were obtained from the available data record, and they were considered independent realizations. Similar considerations yielded 56 and 76 realizations of the $St = 0.3$ and 0.4 modes, respectively, and so on. Further discussion of the data processing is deferred to the results section.

4 Results

Linear PSE assumes the existence of a single unstable normal mode for each $St - M$ pair, whose evolution is tracked in the downstream march. However, if multiple instabilities exist, the appropriate approach is nonlinear PSE, as originally proposed by Herbert (1994). In the latter case, individual unstable initial modes have to be appropriately weighted with complex scalar factors, which are difficult to determine theoretically.

Gudmundsson (2010) applied the parallel-flow linear stability theory (LST) of the NASA PIV data for the same SMC001 - SP7 case (compiled by Bridges & Brown (2004), Opalski et al. (2005)), and reported the existence of two or three unstable eigensolutions for each $St - M$ pair in the near-nozzle region ($x = 0.5$). However, the unstable modes had much lower growth rates at $x = 2$. The LES jet database used in this article does not become fully turbulent until $x \approx 0.7$. Thus, the PSE simulation is initiated from $x_0 = 1.0$. At this station, LST revealed only one unstable eigensolution for each $St - M$ pair. Thus, the use of *linear* PSE is appropriate here.

Figure 1 shows the nature of the PSE eigensolution for a representative frequency ($St = 0.3$). Although 6-fold symmetric structures are evident near the nozzle, the behavior is low-order downstream; e.g., $m = 1$ is dominant in the $M = 1$ solution by $x = 2$. In fact, the structure of the wavepackets evident in the solution is quite similar to those observed in round jets (Gudmundsson & Colonius 2011). Owing to this fact, we will restrict ourselves to the lowest-order azimuthal modes in subsequent portrayals of the PSE solutions.

The PSE model is intended to represent the shape of the most amplified average wavepacket that is, by definition, coherent over the flow domain of the jet. For validation of this shape, we look for a method to determine the most energetic coherent fluctuation in the jet. But this is exactly the purpose of proper orthogonal decomposition (Lumley 1967). Since the pressure field displays the wavepacket character most clearly, the POD modes of pressure are the most relevant in this validation study. The details of this POD technique are documented in Appendix B; the novelty of the present formulation lies in the explicit consideration of the symmetries resulting from the regularly-spaced control devices around the azimuth. As in the PSE analysis in § 2, this not only reduces the computational complexity but also clarifies the flow structures. A similar validation approach was used by Sinha et al. (2014) for LES data in supersonic round jets.

The characteristics of the POD modes of pressure extracted from the LES database are presented in

	$St = 0.2$	$St = 0.3$	$St = 0.4$
$M = 0$	0.78	0.78	0.71
$M = 1$	0.91	0.84	0.86

Table 1: Alignment metric for PSE solutions vis-à-vis first POD modes of pressure in LES database.

Appendix C. In particular, the first POD mode is the most energetic coherent structure found in the flow, and hence is naturally comparable with the PSE solution (Gudmundsson & Colonius 2011, Cavalieri et al. 2013, Sinha et al. 2014).

We present a visual comparison of the PSE eigensolutions with the first POD modes in various $St-M$ pairs in fig. 2. To aid in the comparisons, the PSE solution is rescaled to match the corresponding first pressure POD mode ($\phi_\omega^{M,(1)}$ in Appendix B) by selecting the complex amplitude factors B_ω^M (which is a free parameter in linear PSE) in eqn. (8) with a least-square fit (Sinha et al. 2014)

$$B_\omega^M = \frac{\left\langle \phi_\omega^{M,(1)} \ , \ \breve{p}_\omega^M \right\rangle}{\left|\left|\breve{p}_\omega^M\right|\right|^2}. \tag{11}$$

In the above, $\breve{p}_\omega^M$ is the pressure component of the PSE solution per eqn. (8), but without the B_ω^M factor. The innerproduct (and the norm induced thereof) is defined in eqn. (13).

The PSE solutions display reasonable resemblance with the POD modes, in their least-order azimuthal modes. This is both in regard of the wavelengths (and hence phase speeds) as well as the overall amplitude envelopes. In general, though, the PSE solution appears to decay somewhat earlier than what the data suggests. The comparisons appear better $M = 1$ mode rather than the $M = 0$. All these observations have also been made regarding PSE solutions for round jets, both subsonic and supersonic (Gudmundsson & Colonius 2011, Cavalieri et al. 2013, Sinha et al. 2014).

A more quantitative comparison is performed using the alignment metric defined below (Sinha et al. 2014)

$$\mathcal{A}_\omega^M := \frac{\left|\left\langle \phi_\omega^{M,(1)} \ , \ \breve{p}_\omega^M \right\rangle\right|}{\left|\left|\breve{p}_\omega^M\right|\right| \left|\left|\phi_\omega^{M,(1)}\right|\right|}. \tag{12}$$

The above definition implies that $0 \leq \mathcal{A} \leq 1$. A value close to unity indicates that the PSE solution is structurally equivalent (aligned) to the most coherent wavepacket (first POD mode) found in the flow. Note that the alignment is judged across all coupled azimuthal modes in the solution through the above definition, not just the lowest order one.

The alignment metric is reported for various Fourier mode pairs in table 1. While the qualitative observations made regarding fig. 2 are borne out, the degree of similarity between the predicted wavepackets and those found the data is re-emphasized here.

5 Conclusion

Jet engine exhaust nozzles are being fitted with chevrons or serrations that have been shown to deliver noise attenuation of several dBs. In this article, we propose a stability theoretic model of the coherent wavepackets present in the turbulent shear layer of such jets. These wavepackets have been linked to the dominant aft-angle radiated noise by previous researchers, mainly in jets issuing from round nozzles. Parabolized stability equation (PSE) has been previously demonstrated to deliver a good model in subsonic and supersonic round jets. We extend this model to jets issuing from serrated nozzles. The base flow field data for the stability analysis is the time-averaged mean flow taken from a validated LES database that simulated a Mach 0.9 cold jet issuing from the SMC001 nozzle (the nominal chevron nozzle design tested by Bridges & Brown (2004)).

Explicit use is made of the statistical symmetries resulting from the symmetries in the nozzle geometry. It is thereby explicated that the linear stability problem in the presence of the serrated mean flow couples the lower order azimuthal modes with higher order ones that are separated from it by integer multiples of the number of lobes (6 here). For example, fluctuations in azimuthal mode $m = 1$ are coupled with those in $7, 13, \ldots$ and $-5, -11, \ldots$.

The predicted pressure wavepackets do not differ from those in round jets in their structure downstream, as regards the low order azimuthal modes. However, near the nozzle, the present wavepackets do show the effect of the chevrons impinging on the shear layer in their higher order structure.

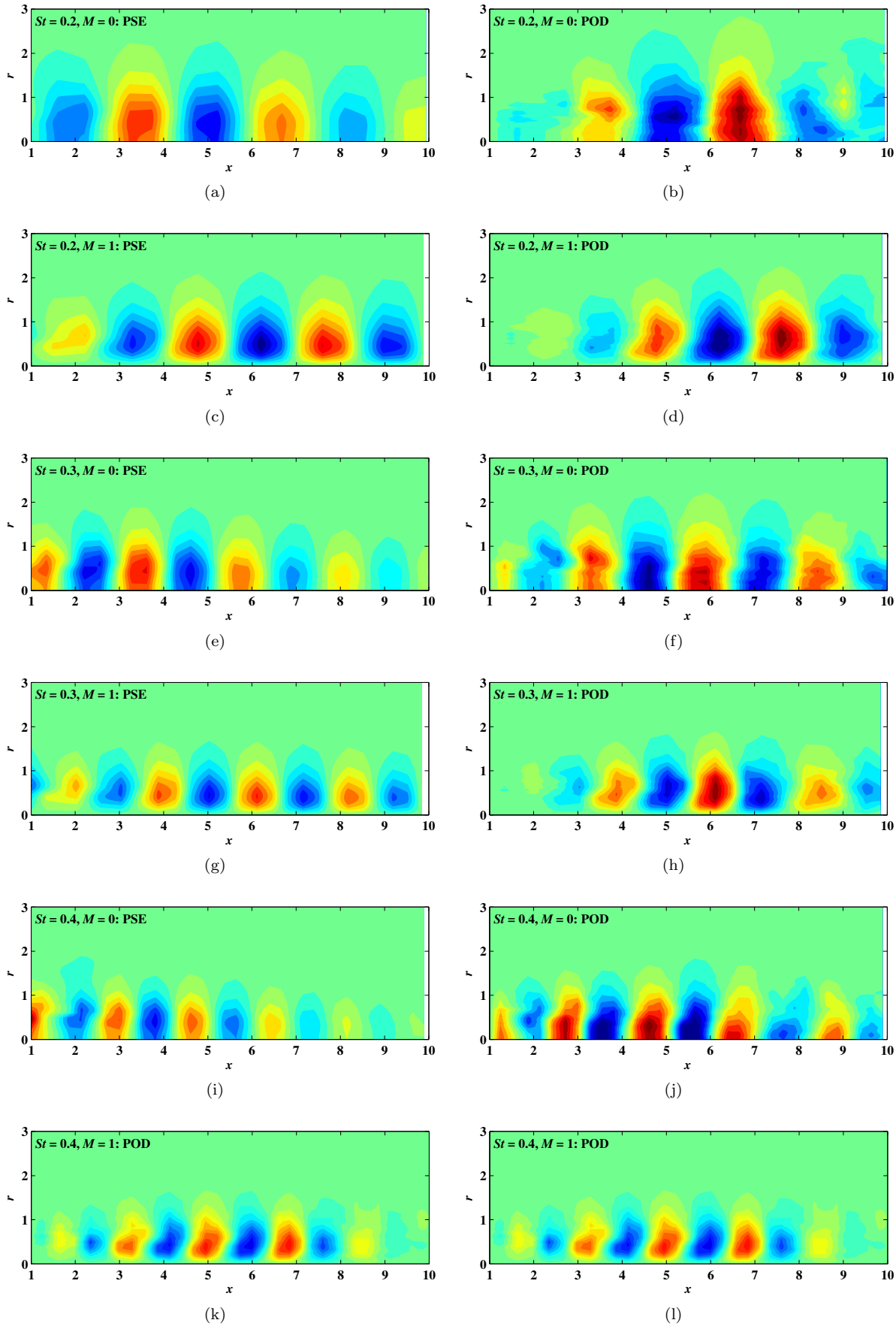

Figure 2: Least-order azimuthal modes of pressure in PSE solution (left panels) compared with corresponding components of first POD mode from LES database (right panels) for $St = 0.2$, 0.3 & 0.4 and azimuthal orders $M = 0$ & 1. Contour levels are identical between each pair of left and right panels, but not across all panels.

The PSE results are validated against the fluctuation data, filtered with proper orthogonal decomposition (POD). Encouraging agreement is observed in terms of both the qualitative and quantitative aspects. We conclude that PSE-predicted instability waves supported by the turbulent mean flow field in high speed jets issuing from serrated nozzles are indeed detectable in the turbulence.

The authors thank Drs. Kristjan Gudmundsson, Arnab Samanta and Daniel Rodríguez for contributing to the development of the PSE code for the round jet. AS acknowledges support from Industrial Research and Consultancy Center of Indian Institute of Technology Bombay, via the seed grant program.

Appendix A Pre-processing the mean flow field

To avoid numerical issues in the PSE calculations, the mean flow data is fitted with a pair of Gaussian functions in a procedure that is an extension of the one used for fitting round jet mean fields (Troutt & McLaughlin 1982). The $m = 0$ mode of the mean axial velocity is fitted with the following function:

$$\hat{\tilde{u}}_{x,0}(x,r) \approx \begin{cases} v_0(x), & 0 < r < s_0(x) \\ v_0(x)\left[\beta(x)\exp\left\{-\dfrac{(r-s_0(x))^2}{(b_{0,1}(x))^2}\right\} + \{1-\beta(x)\}\exp\left\{-\dfrac{(r-s_0(x))^2}{(b_{0,2}(x))^2}\right\}\right], & r \geq s_0(x). \end{cases}$$

The higher azimuthal modes of the mean axial velocity are fitted as

$$\hat{\tilde{u}}_{x,m}(x,r) \approx v_{m,1}(x)\exp\left\{-\frac{(r-s_{m,1}(x))^2}{(b_{m,1}(x))^2}\right\} + v_{m,2}\exp\left\{-\frac{(r-s_{m,2}(x))^2}{(b_{m,2}(x))^2}\right\}.$$

The profile parameters are determined at each x-station by least-squares fitting. The mean specific volume is estimated from these smoothed profiles by the Crocco-Busemann relation (Gudmundsson & Colonius 2011).

The mean radial velocity $\hat{\tilde{u}}_r$ is recovered from $\hat{\tilde{u}}_x$ and $\hat{\tilde{\zeta}}$ by appealing to the compressible mean continuity equation, and assuming that the mean azimuthal velocity $\hat{\tilde{u}}_\theta$ is negligible. This contravenes many researchers (e.g. Alkislar et al. 2007) who have suggested that the streamwise vorticity (and hence $\hat{\tilde{u}}_\theta$) is important for understanding the dynamics of jets issuing from serrated nozzles. However, we used the full mean flow information from LES in separate PSE calculations, and did not notice any significant differences in results, apart from the minor numerical instabilities arising from the non-smooth profiles.

Appendix B POD modes of the serrated jet flow

The complex frequential mode of pressure at frequency ω is denoted $P_\omega(x,r,\theta)$. As explained in § 3, we obtain sufficient realizations of this from the LES data, the kth being denoted $P_\omega^{[k]}$. The inner product for the POD is defined for two fields $P_\omega^{[i]}$ and $P_\omega^{[j]}$ as

$$\left\langle P_\omega^{[i]}\ ,\ P_\omega^{[j]} \right\rangle = \int_{-\pi}^{\pi}\int_{X_1}^{X_2}\int_0^\infty \left\{P_\omega^{[j]}(x,r,\theta)\right\}^\dagger P_\omega^{[i]}(x,r,\theta)\, r\mathrm{d}r\mathrm{d}x\mathrm{d}\theta, \tag{13}$$

where X_1 and X_2 are respectively the upstream and downstream limits of the streamwise domain of interest. For our purposes, $X_1 = 1$ and $X_2 = 10$. With this, the integral eigenvalue (POD) problem in the x, r, θ domain is (Lumley 1967)

$$\int_{-\pi}^{\pi}\int_{X_1}^{X_2}\int_0^\infty r_1^{1/2} E\left[P(x_1,r_1,\theta_1)\, P^\dagger(x_2,r_2,\theta_2)\right] r_2^{1/2} r_2^{1/2}\phi(x_2,r_2,\theta_2)\,\mathrm{d}r_2\mathrm{d}x_2\mathrm{d}\theta_2 = \Lambda r_1^{1/2}\phi(x_1,r_1,\theta_1), \tag{14}$$

where $E(\cdot)$ denotes the expectation over the different realizations, so that the kernel is the 2-point cross-correlation tensor. The eigenvalues Λ are non-negative, and the eigenfunction ϕ corresponding to the largest Λ is the most energetic coherent structure in the data per POD theory. The normalization of the nth POD eigenfunction is such that $\left|\left|\phi^{(n)}\right|\right| = \Lambda^{(n)}$, where $||\cdot||$ is the norm induced by the inner product in eqn. (13). Above we have omitted the ω subscripts and the realization index k for notational convenience. The $r^{1/2}$ weightings are introduced to make the problem Hermitian (Baker 1977).

The serrated flow geometry has L symmetric lobes. Thus, we expect that the cross-correlation will be the same if the reference angle is shifted by $2\pi k/L$ as long as the angular difference between the two correlated

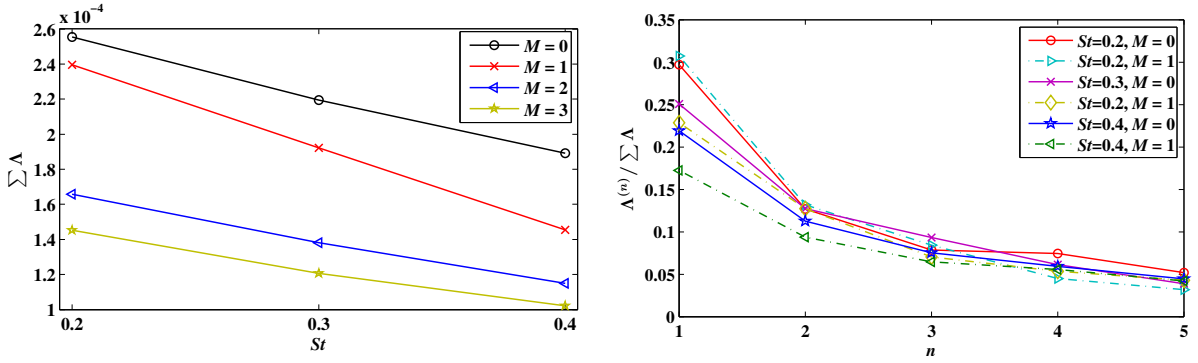

(a) (b)

Figure 3: (a) The total pressure fluctuation 'energy' in the flow domain for the various $St - M$ pairs under consideration. (b) Fraction of pressure fluctuations in the first five POD modes in selected $St - M$ modes.

quantities is maintained. This symmetry is used to 'augment' the data ensemble size, in a manner analogous to POD in the presence of a homogeneous direction (Sirovich 1987). With the definition of azimuthal Fourier transform introduced in § 2, this results in the simplified kernel

$$E\left[P\left(x_1, r_1, \theta + \vartheta\right) P^{\dagger}\left(x_2, r_2, \theta\right)\right] = \sum_{m'=-\infty}^{\infty} \sum_{l=-\infty}^{\infty} E\left[\hat{P}_{m'}\left(x_1, r_1\right) \hat{P}^{\dagger}_{m'-lL}\left(x_2, r_2\right)\right] \mathrm{e}^{\mathrm{i}\left(m'\vartheta + lL\theta\right)}.$$

Substituting this in eqn. (14) and applying azimuthal Fourier transform to the result yields

$$\sum_{l=-C}^{C} \int_{X_1}^{X_2} \int_{0}^{\infty} r_1^{1/2} E\left[\hat{P}_m\left(x_1, r_1\right) \hat{P}^{\dagger}_{m-lL}\left(x_2, r_2\right)\right] r_2^{1/2} r_2^{1/2} \hat{\phi}_{m-lL}\left(x_2, r_2\right) \mathrm{d}r_2 \mathrm{d}x_2 = \Lambda r_1^{1/2} \hat{\phi}_m\left(x_1, r_1\right). \quad (15)$$

This represents the reduced POD problem in the presence of the serrated mean flow. The restriction of the summation to $\pm C$ reflects the limit of the azimuthal grid resolution of the data, or the vanishing of coupling across a large m-range. As an aside, note that for the round jet $L \to \infty$, so that l can only be zero, and we retrieve the fully decoupled set of POD problems as expected.

The structure of the coupled problem is quite similar to the PSE problem in § 2. Invoking analogous arguments, and using the definition of M, we only need to solve for the sets $M \in \{0, 1, \cdots, \lceil (L-1)/2 \rceil\}$. The corresponding POD solutions in (x, r, θ) domain are the $\Lambda_{\omega}^{M,(n)} - \phi_{\omega}^{M,(n)}$ pairs, as in the PSE. Owing to the mirror symmetry of the serrations, the $+m$ and $-m$ will have the same statistics, which is to be used to appropriately augment the expectation operation in the computation of the kernel (Sirovich 1987). In the actual implementation, the equivalent snapshot method is used (Sirovich 1987, Sinha et al. 2014).

Appendix C Characteristics of the POD modes of pressure

It will be recalled that the axial domain of the POD is $x \in [1, 10]$. The total fluctuation energy (as represented by the square norm induced from the inner product defined in eqn. (13)) in this domain indicates the relative importance of the various $St - M$ modes in the turbulence. This energy is equal to the sum of the POD eigenvalues retrieved, per POD theory. The total energy decreases rapidly with increasing azimuthal mode, $M = 0$ and $M = 1$ being distinctly more energetic than the higher azimuthal orders. The pressure fluctuations at higher frequencies are confined over smaller x-regions (see fig. **??**), which accounts for the monotonic decrease in integrated energy with St.

The fraction of total pressure energy represented by the first POD modes of various relevant Fourier modes is shown in fig. 3(b). The first POD mode captures 17 to 30% of the fluctuation energy, across the range of modes depicted. Recalling the large domain of the POD calculation that greatly exceeds the integral length scales of the flow, this attests to very significant coherence for all of the modes depicted.

Although a direct comparison with round jets operated under the same conditions isn't available, a similar POD analysis pursued with LES data of Mach 1.5 round jets (Sinha et al. 2014) is pertinent here. The fractional coherence numbers were approximately double in the latter cases. The lower coherence in the jet issuing from the serrated nozzle studied here is explained by the breaking up of natural large-scale structures by the chevrons impinging on the shear layer.

References

Alkislar, M. B., Krothapalli, A. & Butler, G. W. (2007), 'The effect of streamwise vortices on the aeroacoustics of a Mach 0.9 jet', *Journal of Fluid Mechanics* **578**, 139–169.

Amestoy, P. R., Duff, I. S., LExcellent, J.-Y. & Koster, J. (2001), 'A fully asynchronous multifrontal solver using distributed dynamic scheduling', *SIAM Journal on Matrix Analysis and Applications* **23**(1), 15–41.

Baker, C. T. H. (1977), *The numerical treatment of integral equations*, Clarendon.

Balakumar, P. (1998), Prediction of supersonic jet noises, *in* '36th AIAA Aerospace Sciences Meeting, AIAA Paper 1998-1057'.

Bridges, J. E. & Brown, C. A. (2004), Parametric testing of chevrons on single flow hot jets, *in* '10th AIAA/CEAS Aeroacoustics Conference, AIAA Paper 2004-2824'.

Brown, C. A. & Bridges, J. E. (2003), An analysis of model scale data transformation to full scale flight using chevron nozzles, Technical report, NASA TM-2003-212732.

Cavalieri, A. V. G., Rodríguez, D., Jordan, P., Colonius, T. & Gervais, Y. (2013), 'Wavepackets in the velocity field of turbulent jets', *Journal of Fluid Mechanics* **730**, 559–592.

Crighton, D. G. & Gaster, M. (1976), 'Stability of slowly diverging jet flow', *Journal of Fluid Mechanics* **77**(2), 397–413.

Crow, S. & Champagne, F. (1971), 'Orderly structure in jet turbulence', *Journal of Fluid Mechanics* **48**(3), 547–591.

Day, M. J., Mansour, N. N. & Reynolds, W. C. (2001), 'Nonlinear stability and structure of compressible reacting mixing layers', *Journal of Fluid Mechanics* **446**, 375–408.

Freund, J. B. (1997), Compressibility effects in a turbulent axisymmetric mixing layer, PhD thesis, Stanford University.

Goldstein, M. E. & Leib, S. J. (2005), 'The role of instability waves in predicting jet noise', *Journal of Fluid Mechanics* **525**, 37–72.

Gudmundsson, K. (2010), Instability wave models of turbulent jets from round and serrated nozzles, PhD thesis, California Institute of Technology.

Gudmundsson, K. & Colonius, T. (2007), Spatial stability analysis of chevron jet profiles, *in* '13th AIAA/CEAS Aeroacoustics Conference, AIAA Paper 2007-3599'.

Gudmundsson, K. & Colonius, T. (2011), 'Instability wave models for the near-field fluctuations of turbulent jets', *Journal of Fluid Mechanics* **689**, 97–128.

Herbert, T. (1994), Parabolized stability equations, *in* 'Special Course on Progress in Transition Modelling', number AGARD Rep. No. 793.

Herbert, T. (1997), 'Parabolized stability equations', *Annu. Rev. Fluid Mech.* **29**, 245–283.

Jordan, P. & Colonius, T. (2013), 'Wave packets and turbulent jet noise', *Annu. Rev. Fluid Mech.* **45**, 173–195.

Jordan, P. & Gervais, Y. (2008), 'Subsonic jet aeroacoustics: associating experiment, modelling and simulation', *Experiments in Fluids* **44**(1), 1–21.

Li, F. & Malik, M. R. (1997), 'Spectral analysis of parabolized stability equations', *Computers & Fluids* **26**(3), 279–297.

Lumley, J. L. (1967), The structure of inhomogeneous turbulent flows, *in* A. M. Yaglom & V. I. Tatarsky, eds, 'Atm. Turb. and Radio Wave Prop.', Nauka, Moscow, pp. 166–178.

Mankbadi, R. & Liu, J. T. C. (1984), 'Sound generated aerodynamically revisited: Large-scale structures in a turbulent jet as a source of sound', *Proc. R. Soc. Lond. A* **311**(1516), 183–217.

Mohseni, K. & Colonius, T. (2000), 'Numerical treatment of polar coordinate singularities', *Journal of Computational Physics* **157**, 787–795.

Mollo-Christensen, E. (1967), 'Jet noise and shear flow instability seen from an experimenters point of view', *Journal of Applied Mechanics* **34**(1), 1–7.

Opalski, A. B., Wernet, M. P. & Bridges, J. E. (2005), Chevron nozzle performance characterization using stereoscopic DPIV, *in* '43rd AIAA Aerospace Sciences Meeting and Exhibit, AIAA Paper 2005-444'.

Piot, E., Casalis, G., Muller, F. & Bailly, C. (2006), 'Investigation of the PSE approach for subsonic and supersonic hot jets. Detailed comparisons with LES and linearized Euler equations results', *International Journal of Aeroacoustics* **5**(4), 361–393.

Sinha, A., Rodríguez, D., Brès, G. & Colonius, T. (2014), 'Wavepacket models for supersonic jet noise', *Journal of Fluid Mechanics* **742**, 71–95.

Sirovich, L. (1987), 'Turbulence and the dynamics of coherent structures, Parts I-III', *Quarterly of Applied Mathematics* **XLV**(3), 561–590.

Suzuki, T. & Colonius, T. (2006), 'Instability waves in a subsonic round jet detected using a near-field phased microphone array', *Journal of Fluid Mechanics* **565**, 197–226.

Tam, C. K. W. & Burton, D. E. (1984), 'Sound generated by instability waves of supersonic flows. Part 1. Two-dimensional mixing layers', *Journal of Fluid Mechanics* **138**, 249–271.

Tam, C. K. W. & Chen, P. (1994), 'Turbulent mixing noise from supersonic jets', *AIAA Journal* **32**(9), 1774–1780.

Tanna, H. K. (1977), 'An experimental study of jet noise. Part I: turbulent mixing noise', *Journal of Sound and Vibration* **50**(3), 405–428.

Thompson, K. W. (1987), 'Time dependent boundary conditions for hyperbolic systems', *Journal of Computational Physics* **68**, 1–24.

Troutt, T. R. & McLaughlin, D. K. (1982), 'Experiments on the flow and acoustic properties of a moderate-Reynolds-number supersonic jet', *Journal of Fluid Mechanics* **116**, 123–156.

Xia, H., Tucker, P. G. & Eastwood, S. J. (2009), 'Large-eddy simulations of chevron jet flows with noise predictions', *Int. J. Heat and Fluid Flow* **30**, 1067–1079.

Yen, C. C. & Messersmith, N. L. (1998), 'Application of parabolized stability equations to the prediction of jet instabilities', *AIAA Journal* **36**(8), 1541–1544.